ISSN: 2350-0328

International Journal of Advanced Research in Science, Engineering and Technology

Vol. 9, Issue 10 , October 2022

Synthesis and Application of Binary Metal Oxides for Multifunctional Textiles

Abhishek Kumar Singh*, Kamlesh Panwar

M. Tech., Technical Assistant, Department of Silk Reeling & spinning, Central Silk Technological Research Institute, Bengaluru-560068, India

PhD, Research Scientist, Department of Polyurethanes, Huntsman International (India) Pvt. Ltd., Mumbai-400072, India

ABSTRACT: The application of metal oxides particles in textile is one of the trending arenas of research in the present day. In this work, we report to synthesize ZnO-TiO_2, Al_2O_3-SiO_2, MgO-ZrO_2 and MgO-TiO_2 binary metal oxide particles in molar ratio of 1:4, 1:9, 12:1 and 2:1 respectively. These binary metal oxides were synthesized by sol-gel method and characterized by Dynamic light scattering (DLS), X-ray diffraction (XRD) and Fourier transform infrared spectroscopy (FTIR). Binary metal oxides with particle size ranging from 0.7 to 2.4 µm were obtained. Different formulations were prepared using different combinations of these binary compounds and bentonite powder and were applied on cotton fabric via. padding. Uniform distribution of metal oxides on cotton fabric was confirmed by SEM images. The treated fabrics were evaluated for their thermal behavior while in contact with skin using FLIR thermal sensing camera. Out of various samples prepared, samples AS02 and AS05 showed better far infrared emissive properties due to which the temperature of the skin was observed to increase by almost 0.5 °C and 0.7 °C, respectively. AS04 and AS05 treated fabrics displayed very good UV protection with UPF ratting 30+ and 35+, respectively. AS05 could be used for developing multifunctional fabrics with both far infrared emissive properties as well as high UV protection factor.

KEY WORDS: Binary Metal Oxide, Hydroxyethyl cellulose, bentonite powder, FLIR thermal sensing, UV protection factor.

I. INTRODUCTION

Multifunctional textile materials have very extensive demand worldwide in current time due to their potential applications in the area of self-cleaning, anticorrosion, oil-water separation, UV protective, wrinkle resistant, moisture absorption, antibacterial and fire protective [1-8]. Metal oxides have used in textile material to enhance these functional properties. UV protective and antimicrobial textiles can be produced by using TiO_2, ZnO, SiO_2, CuO and Ag nanoparticles and these metal oxides can also be enhanced wrinkle resistant and self-cleaning properties. Electric conductivity of textiles can be produced by using CuO, clay, Antimony-doped tin oxide, Au, Ag and Cu oxides [9]. Binary metal oxide nanoparticles are produced by combination of two or more metal oxides which give improved function properties on textiles. The different metals having different oxidation states can combine in different ratios to give binary metal oxide nanoparticles. The synthesized binary metal oxide nanoparticles have various physical, morphological and chemical properties that can provide various properties in various applications. In literature, ZrO_2 has been capability to develop FIR finishes for textiles which could be used in both leisure activities and competitive sports areas. Since, various metal oxides have reported to give emissions in FIR range, so, it would be interesting to explore the effect of various combinations of binary metal oxides in imparting FIR properties on fabrics. In this work, various binary metal oxides could be synthesized and applied in combinations with different proportions on cotton fabric. The FIR emitting capability of these treated fabrics could also be explored.

II. RELATED WORKS

Binary metal oxides can be used to impart several functional properties of textile materials. Nano-roughness is generated on textile material by using several binary metal oxides baaed on TiO_2, ZnO, SiO_2 and Au oxide. SiO_2-Al_2O_3 binary metal oxide nanoparticles have been successfully synthesized and applied by pad-dry-cure method on cotton fabrics to impart water repellency [10]. ZnO-SiO_2 has been applied on cotton by using layer by layer deposition method along with octadecyltrimethoxysilane that covered the fabric uniformly and excellent WCA observed [11]. TiO_2-ZnO nanoparticles was applied on cotton fabric that form a transparent photocatalyst nanolayer which gives excellent chemical self-cleaning properties [12]. Ag-TiO_2 nanocomposite was synthesized by sol-gel method and applied on cotton which provides durable self-cleaning activity. Binary meal oxides formed a uniform thin film over the cotton fabric which effectively provides the self-cleaning activity due to photodegradation of stain [13]. TiO_2-Au binary metal oxides on cotton was investigated against the photocatalytic activity in the soler light which exhibited greater photocatalytic

ISSN: 2350-0328
International Journal of Advanced Research in Science, Engineering and Technology
Vol. 9, Issue 10 , October 2022

activity as compared to TiO_2 coated cotton fabric [14]. Synthesized Ag-TiO_2-SiO_2 was applied on textile material which provides excellent self-cleaning properties due to synergetic effect of these three metal oxides [15]. ZnO, Ag, SiO_2, Al_2O_3 and TiO_2 nanoparticles have been coated on cotton by single layer and layer by layer deposition and investigated their antibacterial, self-cleaning and UV-blocking properties [16]. In a literature [17], TiO_2 and ZnO nanoparticles was applied on cotton and cotton/polyester blended woven and knitted fabrics by using pad-dry-cure method for UV protective textiles. SiO_2 coated PVP-capped ZnO nanoparticles was synthesized and applied on wool which reduces absorption of UV radiation on wool by scattering phenomenon and enhance their UV protection [18]. Both uncalcined and calcined Si, Al and K oxides ceramic powder were use for FIR application and they were observed emissivity 0.87 and 0.94 respectively [19]. Another literature reported to the micro-sized metal oxides nanoparticle viz, Zr, Si, Mg, Ca, Zr, S, Fe, Al with ceramic powder were used for FIR application and they were founded average emissivity 0.9 of synthesized material [20].

III. MATERIAL AND METHODS

A) Synthesis of ZnO-TiO_2 binary metal oxide

ZnO-TiO2 binary metal oxide was synthesized by sol-gel method. Zinc acetate and Titanium tetraisopropoxide (TTIP) were used as zinc and titanium precursors respectively in a Ti:Zn molar ratio of 0.05:0.0125 (4:1). The synthesized binary metal oxide was calcined at 700°C for 2 h in muffle furnace [21].

B) Synthesis of Al_2O_3-SiO_2 binary metal oxide

SiO_2-Al_2O_3 binary metal oxide was synthesized by sol-gel method with proportion of 9:1 (Si:Al) molar ratio. Aluminum nitrate nonahydrate (98%) and tetraethyl orthosilicate (TEOS) (98%) were used as aluminum and silica precursor respectively. The synthesized SiO_2-Al_2O_3 binary metal oxide was calcined at 540°C for 3 h in muffle [22].

C) Synthesis of MgO-ZrO_2 binary binary metal oxide

The magnesia–zirconia binary oxide was synthesized by sol-gel and magnesium nitrate (98%) and zirconyl oxychloride (99.9%) were used as precursors during synthesized binary metal oxide. The synthesized binary metal oxide was subjected to calcinate in a muffle furnace at 600°C for 3 h. The resulted particle was found in a Mg:Zr molar ratio of 12:1 [23].

D) Synthesis of MgO-TiO_2 binary binary metal oxide

MgO-TiO_2 binary oxide was synthesized by sol-gel and magnesium nitrate (98%) and titanium dioxide (98%) were used as precursors. The synthesized magnesium-titanium binary metal oxide was subjected to calcinate in a muffle furnace at 600°C for 3 h. The resulted particle was found in a Mg:Ti molar ratio of 2:1 [23].

E) Preparation and application on textiles

Various compositions of binary metal oxides were prepared by mixing different ratios of synthesized binary metal oxides viz. TiO_2-SiO_2, Al2O_3-SiO_2, MgO-ZrO_2, MgO-TiO_2, prior to their application on cotton fabric. The different combinations of metal oxides are summarized in Table 2.1. 2 gm of total weight of these different combinations of binary metal oxides in particular ratios were dispersed in 50 ml of water along with 1.5 gm of Hydroxyethyl cellulose (HEC) and 1 gm of Bentonite powder (Clay) under magnetic stirring at 60°C to make a viscous paste. These samples were coded as AS01 to AS04. In case of AS05, 1.5 gm of Hydroxyethyl cellulose (HEC) and 3 gm of Bentonite powder (Clay) were used along with 2 g of metal oxide powder.

ISSN: 2350-0328

International Journal of Advanced Research in Science, Engineering and Technology

Vol. 9, Issue 10 , October 2022

Table 2.1: Various combinations of binary metal oxides

Sample code	TiO_2-ZnO (%)	Al_2O_3-SiO_2 (%)	MgO-ZrO_2 (%)	MgO-TiO_2 (%)	Hydroxyethyl Cellulose (gm)	Bentonite powder (gm)
	Molar Ratio- 4:1	Molar Ratio- 1:9	Molar Ratio- 12:1	Molar Ratio- 2:1		
Untreated						
AS01	25	25	25	25	1.5	1
AS02	48	2	48	2	1.5	1
AS03	55	5	35	5	1.5	1
AS04	60	5	33	2	1.5	1
AS05	60	5	33	2	3	1

The above viscous paste was applied on cotton fabric by pad-dry-cure method. 17 gm of different combinational binary metal oxides viscous paste was dissolved in 200 ml of di-water to make a 85 gpl (w/v) solution. The cotton fabric samples were padded with the help of padding mangle with 70% pick-up. After padding, 4% add-on was observed. Padded samples were dried at 120°C for 2 min and cured at 160°C for 2 min with the help of drying setting and curing chamber.

IV. EXPERIMENTAL RESULTS

The average particle size of the ZnO-TiO_2 binary metal oxide was characterized using dynamic light scattering technique. The average particle size of the uncalcined ZnO-TiO_2 binary metal oxide was found to be 1563 nm in diameter as shown in Figure 3.1a, which increased to 1848 nm, as shown in Figure 3.1b, after calcination. The average particle size of the uncalcined Al_2O_3-SiO_2 binary metal oxide was found to be 755 nm, as shown in Figure 3.2a, which increased to 874 nm, as shown in Figure 3.2b, after calcination. The average particle size of the uncalcined MgO-ZrO_2 binary metal oxide was found to be 2452 nm in diameter as shown in Figure 3.3a. While the average particle size of the calcined MgO-ZrO_2 binary metal oxide was 2092 nm as shown in Figure 3.3b. The average particle size of the uncalcined MgO-TiO_2 binary metal oxide was found to be 1716 nm in diameter as shown in Figure 3.4a. While the average particle size of the calcined MgO-TiO_2 binary metal oxide was 1722 nm as shown in Figure 3.3b. The results show that the particle size of binary metal oxide viz., ZnO-TiO_2, Al_2O_3-SiO_2, MgO-TiO_2 were smaller after calcination in Table 3.2. It is reported that calcination leads to the production of products with larger particles as a result of sintering and agglomerate formation. This situation was observed for all the binary metal oxide materials except samples MgO-ZrO_2 and MgO-TiO_2. This situation was observed due to densification of MgO particles. MgO reported to control abnormal grain growth of binary metal oxide during calcination [24]. All calcined binary metal oxide systems exhibit monomodal particle size distributions.

Table 3.2: Particle size of binary metal oxide obtained via the sol-gel method

Sample Code	Binary metal oxide	Molar ratio	Temperature of calcination (°C)	Particle size (nm)	
				Uncalcined	Calcined
BMO1	TiO_2-ZnO	4:1	700°C	1563	1848
BMO2	Al_2O_3-SiO_2	1:9	540°C	755	874
BMO3	MgO-ZrO_2	9:1	600°C	2552	2092
BMO4	MgO-TiO_2	2:1	600°C	1716	1722

ISSN: 2350-0328
International Journal of Advanced Research in Science, Engineering and Technology
Vol. 9, Issue 10 , October 2022

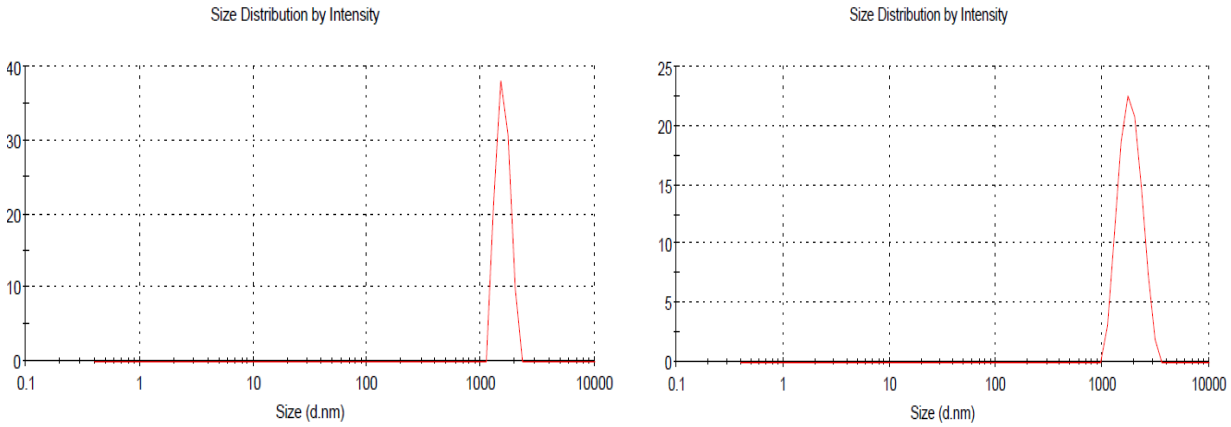

Figure 3.1: Average particle size of $ZnO\text{-}TiO_2$ binary metal oxide, **a.** Uncalcined, **b.** Calcined at 700°C for 2 hrs

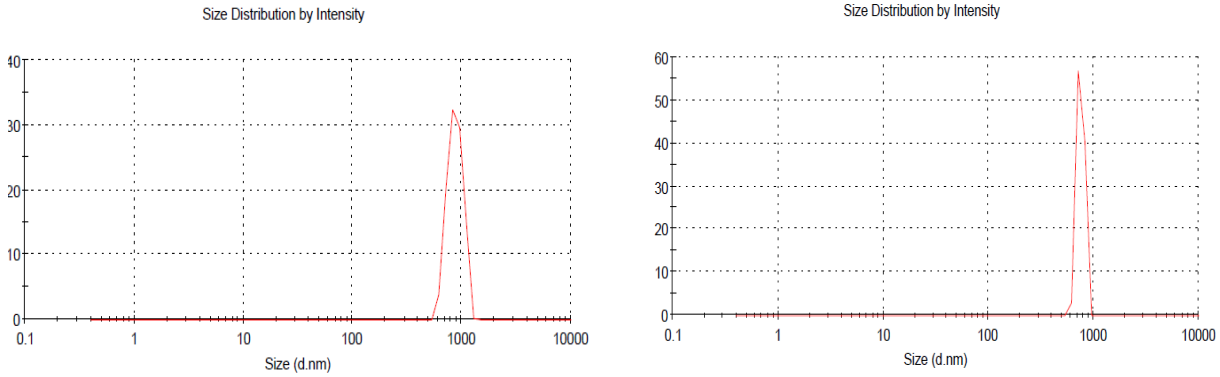

Figure 3.2: Average particle size of $Al_2O_3\text{-}SiO_2$ binary metal oxide, **a.** Uncalcined, **b.** Calcined at 540°C for 3 hrs

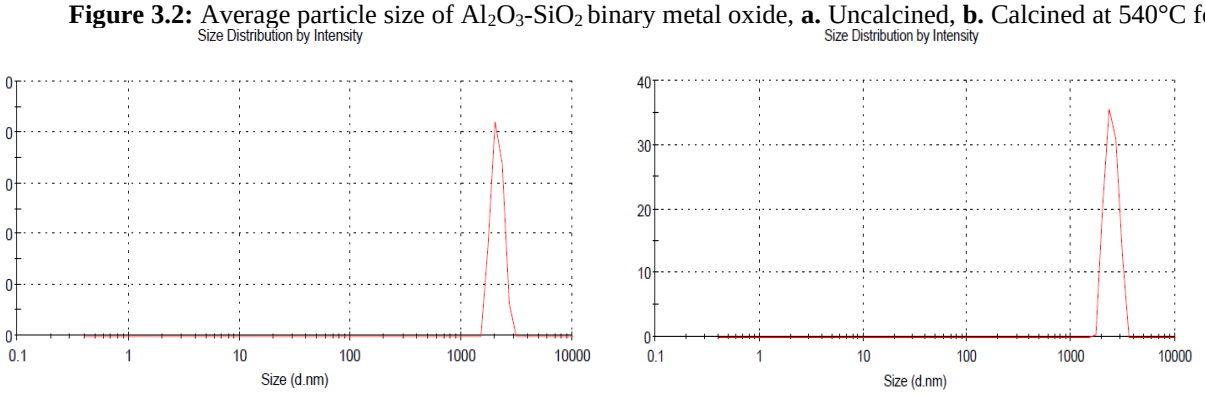

Figure 3.3: Average particle size of $MgO\text{-}ZrO_2$ binary metal oxide, **a.** Uncalcined, **b.** Calcined at 600°C for 3 hrs

ISSN: 2350-0328
International Journal of Advanced Research in Science, Engineering and Technology
Vol. 9, Issue 10 , October 2022

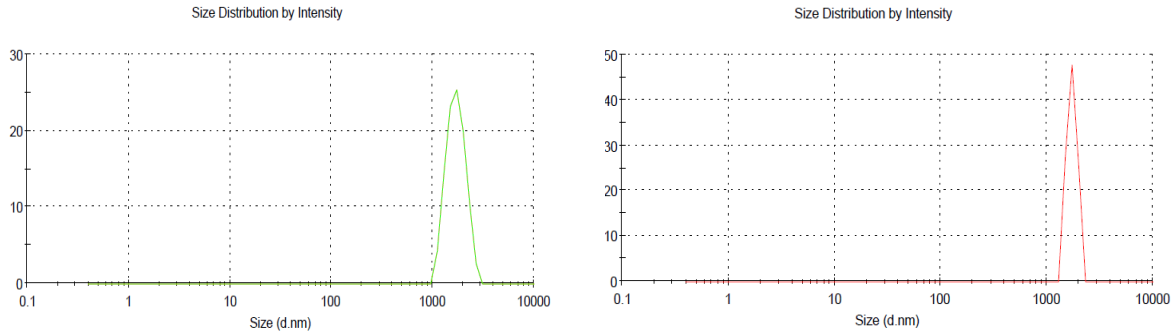

Figure 3.4: Average particle size of MgO-TiO_2 binary metal oxide, **a.** Uncalcined, **b.** Calcined at 600°C for 3 hrs

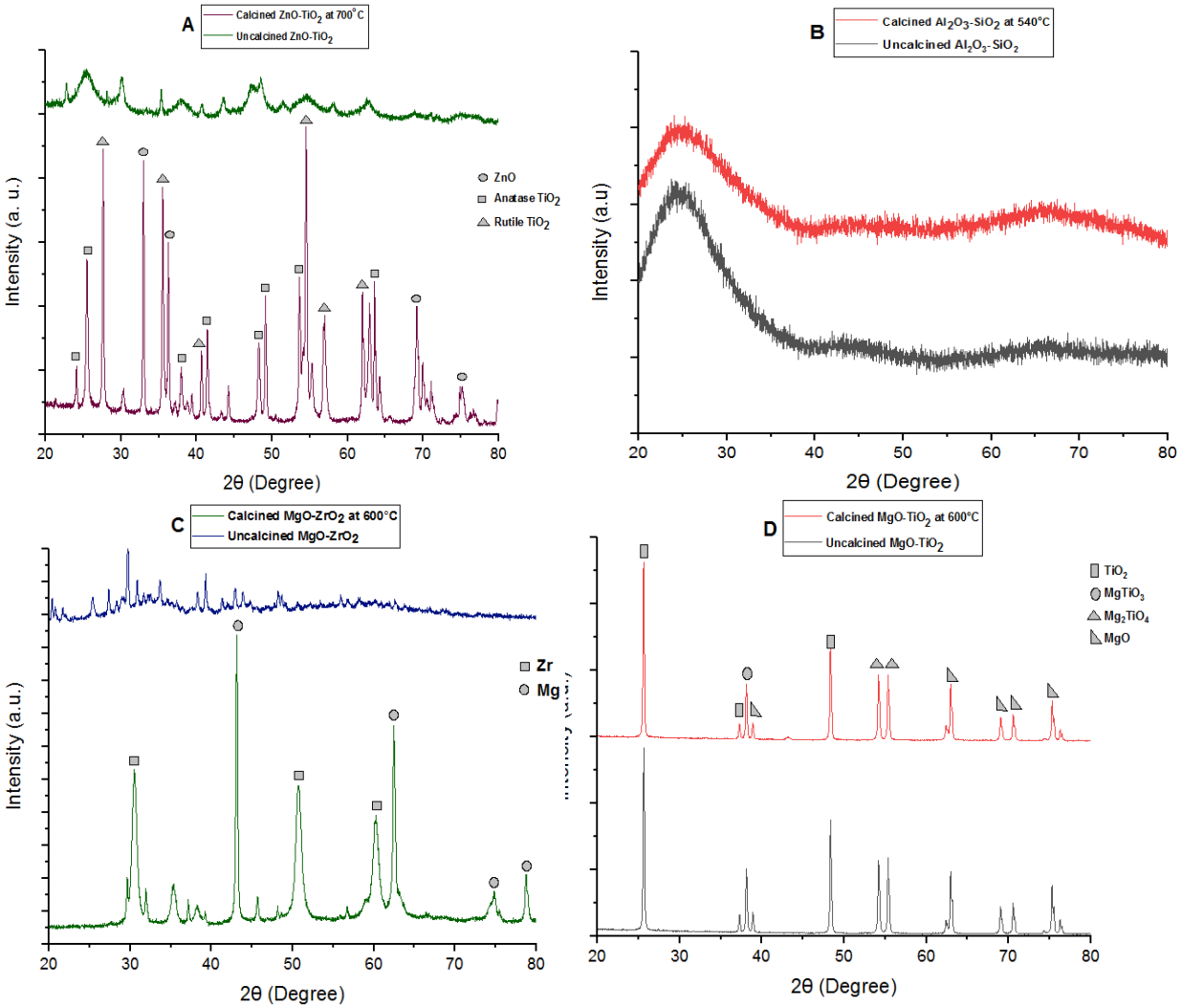

Figure 3.5: XRD analysis of calcined binary powder metal oxides, **(A)** ZnO-TiO_2, **(B)** Al_2O_3-SiO_2, **(C)** MgO-ZrO_2, **(D)** MgO-TiO_2

Figure 3.5 (A) shows XRD pattern of the uncalcined and calcined samples of ZnO-TiO_2 binary metal oxide. The uncalcined sample shows amorphous in nature. XRD pattern of calcined ZnO-TiO_2 sample shows sharp diffraction peak due to formation of crystal structure after calcined at 700°C. From the XRD pattern and corresponding characteristic 2θ values of diffraction peaks, it can be confirmed that TiO_2 particles in the samples are identified as anatase phase according to the JCPDS Card no. 21-1272, for the sharp

ISSN: 2350-0328
International Journal of Advanced Research in Science, Engineering and Technology
Vol. 9, Issue 10 , October 2022

diffraction peaks located at 2θ = 24.8°, 25.47°, 48.2°, 53.6° and 62.8°. Rutile are identified according to the JCPDS Card no. 21-1276, for the sharp diffraction peaks which are found at 2θ = 27.6°, 35.5°, 40.6°, 54.5°, 56.9° and 61.9°. Meantime, several diffraction peaks located at 2θ = 32.9°, 36.2°, 69.1° and 75.2° are also observed zincite phase ZnO particles according to the JCPDS Card no. 36-1451. Therefore, it can be suggested that ZnO-TiO_2 binary samples are the combination of anatase/rutile TiO_2 particles and zincite ZnO particles. In addition, most diffraction peaks in the XRD pattern are sharp and symmetrical Gauss peaks, which further indicate that the particles of TiO_2 and ZnO in the binary samples have high crystallinity [25].
Figure 3.5 (B) displays the X-ray diffraction patterns of the Al_2O_3-SiO_2 binary metal oxides uncalcined and calcined powder samples. The XRD pattern of the Al-Si nanoparticles exhibits a single broad amorphous peak before and after calcination at 540°C. The center of this broad peak is positioned at a lower angle at around 25°. This peak is at an almost similar position to that previously reported for silica-alumina binary oxide [26].

The XRD spectrum of uncalcined and calcined MgO–ZrO_2 binary oxide is shows in Figure 3.5 (C). The uncalcined sample is not show sharp diffraction peak. It shows amorphous structure. After calcined, the XRD pattern was identified with the diffraction peaks located at 2θ = 43.1°, 62.5°, 74.82° and 78.7° which are associated to MgO. ZrO_2 was identified with the diffraction peak located at 2θ = 30.5°, 50.8°, and 60.2°. Monoclinic ZrO_2 and cubic MgO phases were observed in powder diffraction pattern in calcined MgO–ZrO_2 binary oxide at 600°C [27].

Figure 3.5 (D) shows XRD spectrum of both uncalcined and calcined binary MgO–TiO_2. Both the samples were shown crystalline structure. The diffraction peak was observed at 2θ = 25.6°, 37.2°, and 48.3°, which confirmed the anatase phase of TiO_2. Periclase phase MgO was identified the diffraction peak located at 2θ = 38.1°, 63.0°, 69.1°, 70.6° and 75.32°. XRD spectrum also confirmed that MgO–TiO_2 binary compound. The binary compound Geskelite ($MgTiO_3$) and Qandilite (Mg_2TiO_4) were identified the diffraction peak located at 2θ = 38.1° and 54.2°, 55.4° respectively [28].

Figure 3.6 shows the IR spectra of samples BMO1 after calcination. Asymmetric (1713 cm^{-1}) and symmetric carboxylate stretches (1395 and 1258 cm^{-1}) are assigned to titanium oxalate. The presence of additional amounts of zinc causes an increase in the zinc oxalate v_{asym} (COO^-) stretch at 1619 cm^{-1}, relative to its titanium oxalate equivalent at 1719 cm^{-1}. There is also an increase in the v_{sym} (COO^-) stretches of zinc oxalate (1362 and 1317 cm^{-1}), compared to their titanium counterpart (1395 and 1258 cm^{-1}). Peaks at 805 cm^{-1}, representing δ_{asym}(O-C-O) and v(M-O) in IR spectra. Symmetric and asymmetric carboxylate stretches from titanium and zinc oxalate are clearly present in the IR spectra shown. Excess titanium shown strong signals which is representative of zinc oxalate are still clear. This can be explained through the synthesis where zinc acetate is first reacted with oxalic acid to give zinc oxalate before titanium isopropoxide is added. Therefore, TTIP can chelate with unreacted oxalic acid.

FTIR of BM02, occurrence of peak at 1060cm^{-1} corresponds to Si-O-Al bonding confirming the synthesis of structured oxides in Figure 3.7. On the other hand, peaks in the 500 to 800 cm^{-1} region can be attributed to Al-O bonds both in tetrahedral and octahedral coordination observed at 787 cm^{-1}. The peak was observed at 958 cm^{-1}. This band could be associated with Si-OH and/or Al-OH in calcined sample. Other authors associate this band with Si-O-Al bond vibrations because the absorption band of Si-O bonds at 1100 cm^{-1} for amorphous silica is shifted to lower energies by introducing Si-O-Al bonds.

Figure 3.8 shows FTIR spectrum of BM03, the peak obtained at around 624 cm^{-1} was due to the stretching vibration of Zr-O-Zr bond. The peaks observed at 1348 cm^{-1} could be due to Mg-O interaction. The absorption band at 469 cm^{-1} was assigned to the Zr-O vibration. The characteristic bands were observed at 599, 569 and 532 cm^{-1} for monoclinic zirconia and 514 cm^{-1} for tetragonal zirconia. For zirconia, shifts in wavenumber for the tetragonal and monoclinic phase have been reported in binary oxides prepared by the addition of divalent or trivalent oxides.

FTIR spectra of the BM04 calcined at 600°C is displayed in Figures 3.9. The bands at 1637 cm^{-1} are designated to the C-O flexion mode associated to the formation of intermediate compounds as magnesium oxalates. At 1088 cm^{-1}. The strong Mg-O stretching bond is observed at 700 cm^{-1}.

Spectra showed characteristic peaks below 1100 cm^{-1} the peaks obtained with the effect of C = O bond is due to the possible stretching bond of Ti-O-Mg. The peak observed at 1162, 1109, 1032 cm^{-1} could be due to possible stretching bands of Ti-O-Mg. These peaks are attributed to the formation of new metal-oxygen bonds of -O-Ti-O-Mg-O within the structure. The strong Mg-O stretching bond was observed at 662 cm^{-1}. Ti–O–Ti bond vibrations were found at 554 and 509 cm^{-1}.

The SEM analysis of various compositions of binary metal oxides treated cotton fabric were done to observe the surface morphology of the metal oxide particles and their deposition on fabric. As shown in Figure 3.10, the various binary oxides have an irregular or slightly spherical morphology. Surface of untreated cotton (Figure 3.10-A) was observed to be smooth. However, in case of treated fabrics, the SEM analysis shows uniform distribution of binary metal oxides on the surface of cotton fabric.

ISSN: 2350-0328
International Journal of Advanced Research in Science, Engineering and Technology
Vol. 9, Issue 10 , October 2022

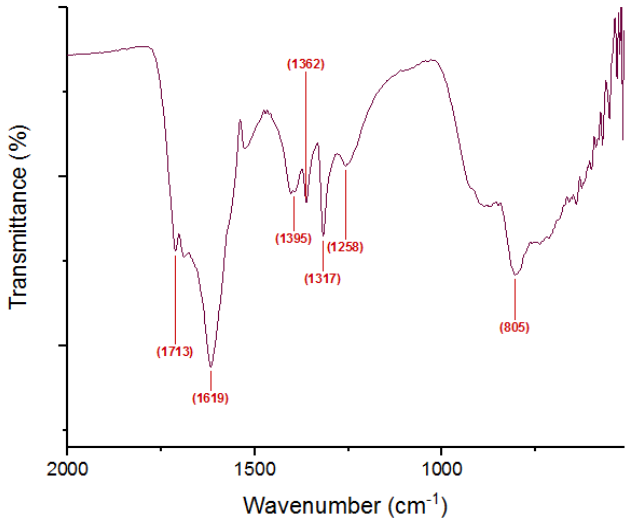

Figure 3.6: FTIR spectra of BM01

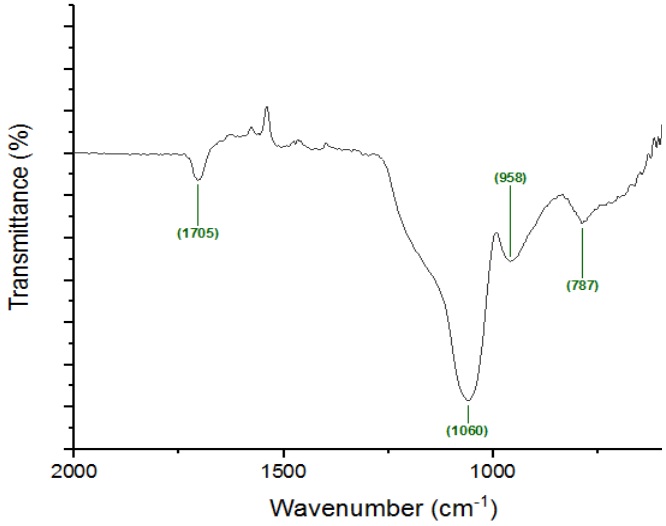

Figure 3.7: FTIR spectra of BM02

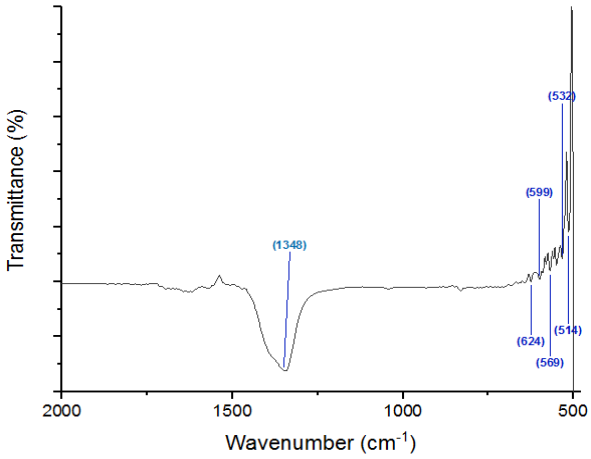

Figure 3.8: FTIR spectra of BM03

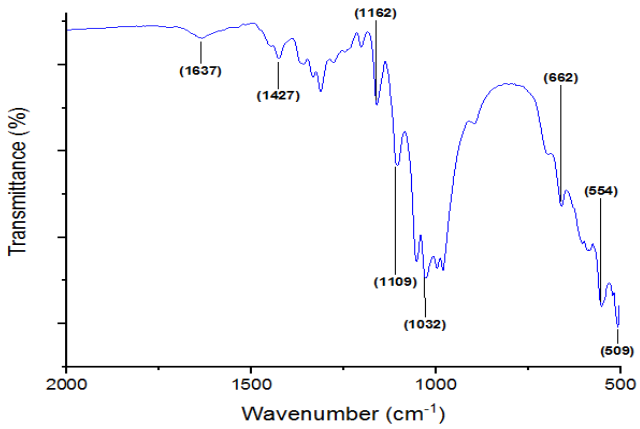

Figure 3.9: FTIR spectra of BM04

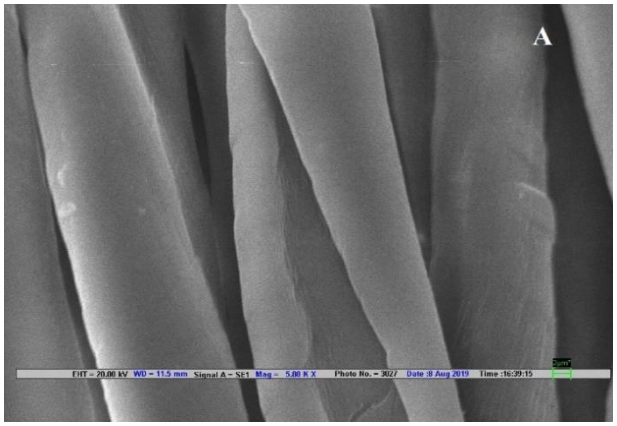

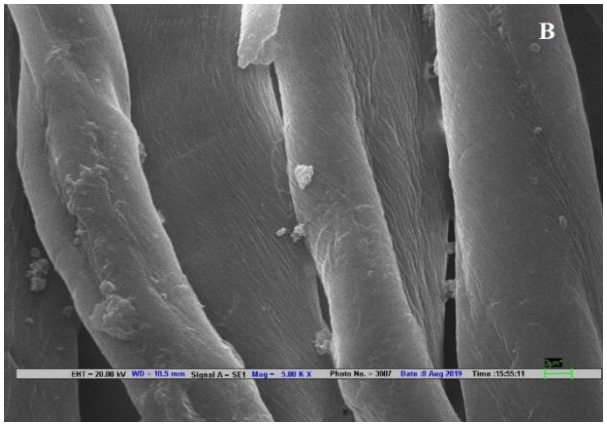

ISSN: 2350-0328
International Journal of Advanced Research in Science, Engineering and Technology
Vol. 9, Issue 10 , October 2022

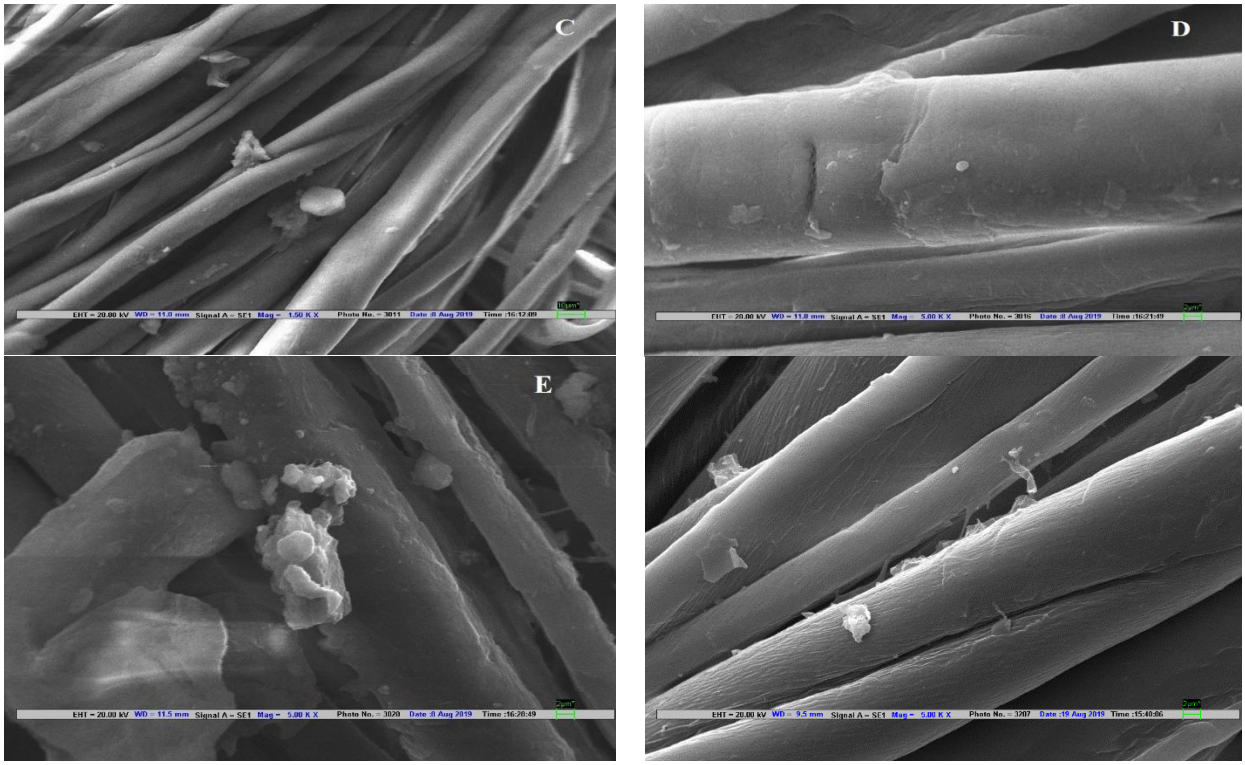

Figure 3.10: SEM images of cotton fabrics, (A) Untreated (UT), (B) AS01, (C) AS02, (D) AS03, (E) AS04, (F) AS05

Table 3.3 shows the thermal behavior of human body while exposed to FIR fabric. Results show that there is no change in the skin temperature when it is covered with untreated cotton fabric for 30 min. However, samples AS01, AS03 and AS04 displayed an increase in body temperature by around 0.2°C, 0.1°C and 0.3°C, respectively, as shown in Figure 3.11. These fabric samples could have low efficiency to emit far infrared rays which could mainly be due to low proportion of Zr based metal oxide in these compositions. Interestingly, samples AS02 and AS05 shows significant increase in body temperature i.e. 0.5°C and 0.7°C, respectively. These fabric samples have potential to work as FIR fabrics since the temperature difference should be at least 0.5 °C.

Table 3.3: Thermal behavior of body against IR via FLIR sensing camera

Sample Code	Initial body temperature before covered by fabric sample (°C)				Body temperature after covered by fabric sample for 30 min (°C)				Difference in body temperature (°C)
	Reading 1	Reading 2	Reading 3	Average	Reading 1	Reading 2	Reading 3	Average	
UT	35.5	35.4	35.4	35.4	35.4	35.4	35.5	35.4	0.0
AS01	35.5	35.5	35.3	35.4	35.8	35.7	35.4	35.6	0.2
AS02	35.0	34.9	34.9	34.9	35.4	35.4	35.6	35.5	0.5
AS03	34.9	34.8	34.8	34.8	34.1	35.2	35.4	34.9	0.1
AS04	34.9	35.2	35.3	35.1	35.6	35.4	35.3	35.4	0.3
AS05	34.7	35	35.1	34.9	35.7	35.7	35.4	35.6	0.7

UPF was also measured for the treated fabrics and compared with the untreated one. The results shown that UPF of the untreated fabric is very low i.e. 9.3. Samples AS01 and AS02 show moderate UPF values 16.1 and 19.2, respectively, as shown in Table 3.4. This is due to the presence of nanomaterials such as TiO_2 and ZnO. The UV absorption is the native property of titanium dioxide. TiO_2 and ZnO are a kind of semiconductor oxide with a large band gap between its low-energy valence band and its high-energy conduction band. Treated fabric samples AS04 and AS05 displayed very good UV protection as compared to other samples. This is due to the presence of higher proportion of ZnO and TiO_2 on to the fabric. In term of UVA and UVB, treated fabric samples AS04 and AS05 shows significant results as compared to other samples and are able to block more UV light than other samples.

Table 3.4: UPF for the different samples for UV-A (315–400 nm) and UV-B (290– 315 nm) radiation

ISSN: 2350-0328
International Journal of Advanced Research in Science, Engineering and Technology
Vol. 9, Issue 10 , October 2022

Sample code	UPF	UPF Class	UPF rating	Mean UVR (%T)	Mean UVA (%T)	Mean UVB (%T)
UT	9.3	Not rateable	5+	10.5	12.3	3.4
AS01	16.1	Moderate	15+	6.3	7.5	1.7
AS02	19.2	Moderate	15+	5.2	6.1	1.6
AS03	22.2	High	20+	4.7	5.7	0.9
AS04	36.1	Very High	35+	3.0	3.5	0.9
AS05	31.6	Very High	30+	3.3	3.8	1.1

Table 3.5 shows the time of water droplet absorption on the untreated and binary metal oxide treated fabrics. All the treated fabrics shows water absorbency almost similar to untreated fabric. Whiteness index of samples was measured to observe if there is any change in whiteness of samples in Table 3.4. It can be seen that whiteness of fabric reduces when binary metal oxides were applied on the fabric. Fabric sample AS05 shows lower whiteness index i.e. 89.07 as compared to other samples. Bending length of the samples was measured and results are reported in Table 3.5. It can be seen from the data that bending length reduces when fabric is treated with binary metal oxides. Treatments lead to some increase in the stiffness of fabric. This could mainly be due to the presence of significant amounts of metal oxides on the surface of treated fabrics.

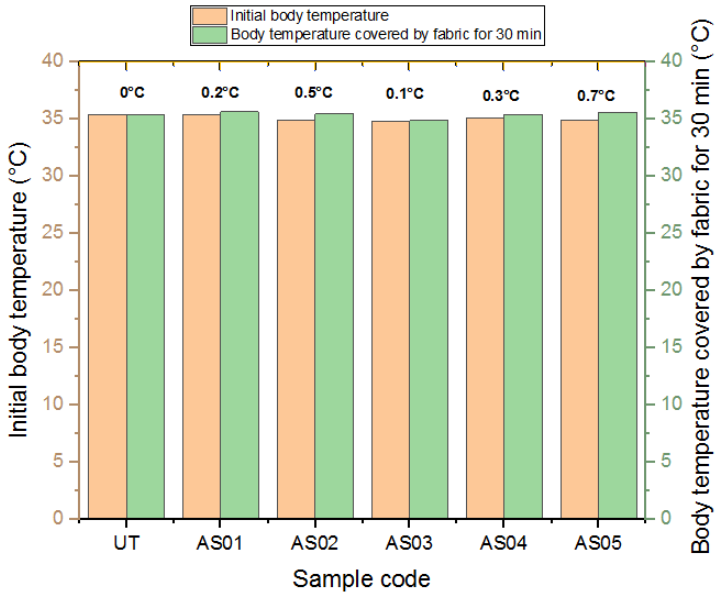

Figure 3.11: Thermal behavior of human body against IR via FLIR sensing camera

Table 3.5: Different properties of fabric treated with binary metal oxide

Sample code	Water absorbency	Bending length	Whiteness inde
	sec	cm	
UT	9	3.7	97.87
AS01	12	3.9	93.94
AS02	8	3.9	94.09
AS03	6	4.0	93.54
AS04	7	3.9	93.97
AS05	7	4.2	89.07

ISSN: 2350-0328
International Journal of Advanced Research in Science, Engineering and Technology
Vol. 9, Issue 10 , October 2022

V. CONCLUSION

The binary metal oxides of ZnO-TiO_2, Al_2O_3-SiO_2, MgO-ZrO_2 and MgO-TiO_2 were prepared by the sol-gel method. The synthesized binary metal oxides were observed to be amorphous in nature and their particle size varied from 0.7 to 2.4 µm. These particles were calcined to form crystalline structures and then applied on cotton fabrics in different combinations of binary metal oxides. The crystalline structure of these calcined metal oxides were studied by XRD. FTIR analysis further confirmed the successful synthesis of the binary metal oxides. The binary metal oxides in different combinations were applied on cotton fabric and studied for the thermal behavior on human body against infrared ray. Treated fabric samples AS02 and AS05 displayed good far infrared properties with body temperature increased by almost 0.5°C and 0.7°C, respectively, after 30 min. AS04 and AS05 showed high UPF with rating 35+ and 30+, respectively. The treated fabrics maintained their water absorption behavior similar to untreated fabric, with slight effect on bending strength and whiteness index of the fabric. Out of various samples prepared, AS05 could be used for multifunctional textiles with good far infrared emissivity and high UV protection factor.

REFERENCES

[1] Yang Z, Wang L, Sun W, Li S, Zhu T, "Superhydrophobic epoxy coating modified by fluorographene used for anti-corrosion and self-cleaning", Appl Surf Sci, 401, pg. no: 146-155, 2017.
[2] Xiao F, Yuan S, Liang B, Li G, Pehkonen SO, "Superhydrophobic CuO nanoneedle-covered copper surfaces for anticorrosion", J Mater Chem A, 3, pg. no: 4374–4388, 2015.
[3] Xu Z, Zhao Y, Wang H, Zhou H, Qin C, "Fluorine-Free Superhydrophobic Coatings with pH-induced Wettability Transition for Controllable Oil-Water Separation" ACS Appl Mater Interfaces, Vol. 8, pg. no: 5661–5667, 2016.
[4] Stankovic S B, Popovic D, Poparic G B and Bizjak M, "Ultraviolet Protection Factor of Gray-state Plain Cotton Knitted Fabrics", Text. Res. J., Vol. 79, pg. no: 1034-1042, 2009.
[5] Hafeezullah Memon, Sohail Yasin, Nazakat Ali Khoso, Samiulah Memon, "Study of wrinkle resistant, breathable, anti-uv nanocoated woven polyester fabric", Surface Review and Letters, Vol 23, Issue 3, 1650003, 2016.
[6] Kelem Tiessasie Yilma, Derseh Yilie Limeneh, "Review on Moisture Management Finish: Mechanism and Evaluation", Journal of Natural Fibers, pg. no: 1-9, 2021.
[7] Pal S, Mondal S, Maity J, "In situ generation and deposition of ZnO nanoparticles on cotton surface to impart hydrophobicity: investigation of antibacterial activity". Mater Technol., Vol. 33, pg. no: 555-562, 2018.
[8] Pal A, Samanta A K, Bagchi A, Samanta P, Kar T P, "A Review on Fire Protective Functional Finishing of Natural Fibre Based Textiles: Present Perspective", Curr Trends Fash Techn Text Eng, Vol 7, Issue 1, pg. no: 555705, 2020.
[9] Shagufta Riaz, Munir Ashraf, Tanveer Hussain, Muhammad Tahir Hussain, Abdur Rehman, Amjed Javid, Kashif Iqbal, Abdul Basita, Humera Aziz, "Functional finishing and coloration of textiles with nanomaterials", Color. Technol., Vol 0, pg. no: 1–20, 2018.
[10] Hao L F, An Q F, Xu X, Wang Q J, "Synthesis of fluoro-containing superhydrophobic cotton fabric with washing resistant property using nano-SiO_2 sol-gel method", Adv. Mater. Res., Vol. 121–122, pg. no: 23-26, 2010.
[11] Wang L, Zhang X, Li B, Sun P, Yang J, Xu H, Liu Y, "Superhydrophobic and Ultraviolet-Blocking Cotton Textiles", ACS Appl. Mater. Interfaces, Vol. 3, pg. no: 1277-1281, 2011.
[12] Herrmann J M, "Photocatalysis fundamentals revisited to avoid several misconceptions", Appl. Catal. B: Environ., Vol. 99, pg. no: 461–468, 2010.
[13] Uddin M J, Cesano F, Scarano D, Bonino F, Agostini G, Spoto G, Bordiga S, Zecchina A, "Cotton textile fibres coated by Au/TiO_2 films: Synthesis, characterization and self-cleaning properties", J. Photochem. Photobiol. A Chem., Vol. 199, pg. no: 64-72, 2008.
[14] Montazer M, Behzadnia A, Moghadam M B, "Superior self-cleaning features on wool fabric using TiO_2/Ag nanocomposite optimized by response surface methodology", J. Appl. Polym. Sci., Vol. 125, pg. no: 356-362, 2012.
[15] Wang R, Wang X, Xin J H, "Effect of Graphene Oxide on the Properties of Its Composite with Polyaniline", ACS Appl. Mater. Interfaces., Vol. 2, pg. no: 821-828, 2010.
[16] Ugur S S, Sarusik M, Aktas A H, Ucar M C, Erden E, "Modifying of Cotton Fabric Surface with Nano-ZnO Multilayer Films by Layer-by-Layer Deposition Method", Nanoscale Res. Lett., Vol. 5, pg. no: 1204-1212, 2010.
[17] Zhang M, Tang B, Sun L, Wang X, "Reducing photoyellowing of wool fabrics with silica coated ZnO nanoparticles", Text. Res. J., Vol. 84, pg no: 1840-1848, 2014.
[18] Amir Kajbafvala, Mohammad Reza Shayegh, Mahyar Mazloumi, Saeid Zanganeh, aidin Lak, Matin Sadat Mohajerani, S.K. Sadrnezhaad, "Nanostructured sword-like ZnO wires: rapid synthesis and characterization through a microwave-assisted route", J. Alloys Comp., Vol. 469, pg. no: 293- 297, 2009.
[19] Ramachandran T, Rajendrakumar K, Rajendran, "Antimicrobial textiles-an overview, R. IE (I) Journal-TX, Vol. 84 (2), pg. no: 42-44, 2004.
[20] Kim, Soon Young, Yoonkyoung Kim, Ki Tae Kwon, Tae Heui Kim, "Effect of Far infrared Rays emitted from the calcined Ceramics on Ethylene Production in Mungbean Hypocotyls", J. Plant Biol. Vol. 41(4), pg no: 298-303, 1998.
[21] Yoshihiko Matsumoto, Keisuke Mita, Keiji Hashimoto, Takashi Tokoroyama, "Preparation of silica-alumina catalyst by the sol-gel method and its activity for the Diels-Alder reaction of isoprene and acrylaldehyde." Applied Catalysis A: General, 131, LI-L6, 1995.
[22] Maria A. Aramendia, Victoriano Borau, Cesar Jimenez, Alberto Marinas, Jose M. Marinas, Jose A. Navio, Jose R. Ruiz, Francisco J. Urbano, "Synthesis and textural-structural characterization of magnesia, magnesia–titania and magnesia–zirconia catalysts." Colloids and Surfaces A: Physicochem. Eng. Aspects, Vol. 234, pg. no:17–25, 2004.
[23] Mohanraj V J, Chen Y, "Nanoparticles-A Review", Trop. J. Pharm. Res., Vol. 5, pg. no. 561-573, 2006.
[24] Nicholas T. Nolan, Michael K. Seery, Suresh C. Pillai, "Crystallization and Phase-Transition Characteristics of Sol-Gel-Synthesized Zinc Titanates", Chem. Mater. Vol. 23, pg. no:1496–1504, 2011.
[25] Liqin Wang, Xiujun Fu, Yang Han, E. Chang, Haitao Wu, Haiying Wang, Kuiying Li, Xiaowen Qi, "Preparation, Characterization, and Photocatalytic Activity of TiO_2/ZnO Nanocomposites", Journal of Nanomaterials, Article ID 321459, pg. no:1-6, 2013.

ISSN: 2350-0328

International Journal of Advanced Research in Science, Engineering and Technology

Vol. 9, Issue 10 , October 2022

[26] Kyungsun Song, Wonbaek Kim, Sangwon Park, Jun-Hwan Bang, Jeongyun Kim, Ji-Whan Ahn, "Preparation of Silica-Alumina Nanoparticles via Blast-Furnace Slag Dissolution in Low-Concentration Acetic Acid for Carbonation", Vol. 7, pg. no: 206-218, 2017.
[27] Manoj B. Gawande, Paula S. Branco, Kalpesh Parghi, Janhavi J. Shrikhande, Rajesh Kumar Pandey, C. A. A. Ghumman, N. Bundaleski, O. M. N. D. Teodorod, Radha V. Jayaramb, "Synthesis and characterization of versatile MgO–ZrO_2 mixed metal oxide nanoparticles and their applications", Catal. Sci. Technol., Vol. 1, pg. no: 1653–1664, 2011.
[28] Lopez T, Hernandez-Ventura J., Aguilar D H, Quintana P., "Thermal Phase Stability and Catalytic Properties of Nanostructured TiO_2-MgO Sol–Gel Mixed Oxides", Journal of Nanoscience and Nanotechnology, Vol. 8, pg. no: 6608–6617, 2008.